Vegetatio **80**: 71–89, 1989

Accuracy of the AVHRR Vegetation Index as a predictor of biomass, primary productivity and net CO_2 flux

Elgene O. Box[1], Brent N. Holben[2] & Virginia Kalb[2]
[1]*Geography Department, University of Georgia, Athens, GA 30602, USA;* [2]*National Aeronautics and Space Administration, Goddard Space Flight Center, Greenbelt, MD 20771, USA*

Accepted 7.11.1988

Keywords: Evapotranspiration, Field measurement, Global geography, Greenness index, NDVI, Radiometer, Satellite calibration, Simulation data

Abstract

The Normalized Difference Vegetation Index (*NDVI*) or 'greenness index', based on the Advanced Very High Resolution Radiometer (AVHRR) aboard the NOAA-7 satellite, has been widely interpreted as a measure of regional to global vegetation patterns. This study provides the first rigorous, quantitative evaluation of global relationships between the *NDVI* and geographically representative vegetation data-bases, including field metabolic measurements and carbon-balance results from global simulation models. Geographic reliability of the *NDVI* is judged by comparing *NDVI* values for different surface types with a general global trend and by statistical analysis of relationships to biomass amounts, net and gross primary productivity, and actual evapotranspiration. *NDVI* data appear to be relatively reliable predictors of primary productivity except in areas of complex terrain, for seasonal values at high latitudes, and in extreme deserts. The strength of the *NDVI*-productivity relationship seems comparable to that of earlier climate-based productivity models. Little consistent relationship was found, across different vegetation types, between *NDVI* and biomass amounts or net biospheric CO_2 flux.

Abbreviations: AET = Actual Evapotranspiration, AVHRR = Advanced Very High Resolution Radiometer, GPP = Gross Primary Production, GVI = Global Vegetation Index, NDVI = Normalized Difference Vegetation Index, NPP = Net Primary Production

Introduction

Recent studies have shown various relationships between remotely sensed spectral signals and biosphere patterns, from landscape to global scale (e.g. Kumar & Monteith 1981; Johannsen & Sanders 1982; Botkin *et al.* 1984; AIBS 1986; Fung *et al.* 1987). In particular, the Advanced Very High Resolution Radiometer (AVHRR) aboard the NOAA-7 satellite has been useful for large-area studies because the orbital characteristics permit complete global coverage within relatively short periods of time (Townshend & Tucker 1984). The AVHRR includes channels in the green (0.58–0.68 μm) and near-infrared (0.725–1.1 μm) wavelengths, corresponding respectively to strong light absorption by chlorophyll (i.e. 'greenness') and spongy mesophyll leaf structure (Justice *et al.* 1985). AVHRR signals are interpreted for analysis of biosphere patterns by means of the Normalized Difference Vegetation Index (*NDVI*), or

'greenness index', a normalized ratio of the two channels which contrasts the two signals and effectively expresses the degree of pixel greenness (Tucker 1979; Tarpley *et al.* 1984). Whereas Thematic Mapper and other sensors may have finer spatial resolution (pixel size), making them more useful for landscape-level work, monthly and annually composited *NDVI* data appear to represent the most useful methodology currently available for monitoring vegetation and related phenomena at global scale (Goward *et al.* 1985; Tucker & Sellers 1986).

Pixel greenness is interpreted as indicating the presence of chlorophyll. Thus, *NDVI* was interpreted originally as a measure of 'green leaf biomass', based on experience mainly with crops and grasslands (Tucker 1980). Annually integrated *NDVI* was shown by Goward *et al.* (1985) to be related to biome averages of annual *NPP*. As an example of the potential usefulness of the *NDVI*, Tucker *et al.* (1985a, 1985b; see also Justice 1986) constructed monthly greenness images for Africa in 1981 and 1982 which graphically show the advance and retreat of the tropical summer wet season and year-to-year differences in surface greenness, which they interpreted as primary production. These African images, however, involve large areas of savanna and deciduous woodland, in which the highly seasonal development of green plant parts and productivity is better captured by a greenness sensor than may be the case in other vegetation types. It has also been suggested that *NDVI* correlates well with seasonal variations in atmospheric CO_2 concentrations (Tucker *et al.* 1986) and fluxes (Fung *et al.* 1987).

Although the *NDVI* appears to be a useful index of some surface phenomena, it is still not certain just what biological phenomena the *NDVI* actually represents. The purpose of this study is to evaluate the significance and geographic variability of the *NDVI* by comparing it with geographically representative sets of biomass and primary production data representing the full range of terrestrial vegetation structures. This involves available field measurements of total above and below-ground biomass and primary production (about 100 valid sites worldwide) as well as bioclimatic data and bioclimatically simulated primary productivity and net CO_2 flux (about 1000 sites for more complete global coverage). The global *NDVI* data are analyzed geographically and compared with the spatially corresponding biosphere data, including monthly patterns. Special effects resulting from vegetation structure, seasonal differences, and high latitude are also noted. This study differs from previous work by being the first to include all major landscape types worldwide, use site biological measurements directly, involve bioclimatic data, use simulated data for the full carbon balance, analyze *NDVI*-biosphere relationships geostatistically, and provide a geographic analysis of discrepancies.

Vegetation metabolism and modeling attempts

Primary production by vegetation represents the basis of ecological energetics. Net primary production (or productivity, i.e. the rate of production) is the resultant of photosynthetic energy fixation (gross primary production, *GPP*) and use of stored energy for maintenance and growth (respiration, *R*), as given by the relation

$$GPP - R = NPP \qquad (1)$$

in which all three components represent amounts of biomass or energy or carbon equivalents. Recent evidence suggests that these basic metabolic processes of vegetation are controlled by ambient environmental conditions, especially climatic factors at broader scales. Gross production generally increases with warmth and water availability (both temporally and geographically), as long as sunlight, nutrients, developed leaf area, and other factors are not limiting (Kira 1975; Lieth & Box 1977). Respiration, on the other hand, appears to be mainly an exponentially increasing function of ambient temperature, at least over the range 0° to 40 °C, and appears to increase almost linearly (saturating somewhat) with increasing amounts of live standing biomass. These relationships are well described in various summaries (e.g. Moeller 1945, 1954; Hozumi *et al.* 1969; Odum 1971; Shidei & Kira 1977; Salisbury & Ross 1978; Waring & Schlesinger 1985) and model descriptions (Shugart 1984; King 1986; Fung *et al.* 1987; Box 1988), and appear to hold for monthly as well as annual values.

Annual *NPP* also appears to increase with warmth and wetness (Major 1963; Rosenzweig 1968; Lieth & Box 1972) but becomes a smaller fraction of annual GPP in warmer regions, since respiration increases faster with higher temperatures than does GPP (Kira 1975; Box 1978). Annual *NPP* represents a net energy gain for the vegetation. Outside the growing season, however, photosynthesis may be negligible while respiration continues, leading to periods during which *NPP* may in fact become a net primary 'deduction' of stored biomass energy. This loss of biomass (not litterfall) by living vegetation, outside the growing season, has been measured both for plants and for whole vegetation stands (e.g. Houghton 1987a, 1987b; Dwivedi 1971).

Biomass structure is the result of biomass accumulation over time. The energy gained by *NPP* is partitioned as follows:

$$NPP = LF + \Delta B + H \quad (2)$$

where LF represents the biomass discarded periodically (litter, i.e. dead leaves, twigs, roots, etc.), ΔB is the permanent component (an increment to the standing live biomass), and H represents the biomass lost to herbivory or harvesting. Annual biomass increments are typically largest in early mid-succession and decrease thereafter (though small annual increments may continue for a very long time). The greatest accumulations of standing biomass occur in the tall 'temperate rainforests' of cool, moist climates such as windward mountains in the northwestern USA, Japan, or New Zealand (Cannell 1982). Primary tropical rainforests also have high biomass accumulations. Low biomass accumulations occur, of course, in deserts, grasslands, polar and alpine vegetation, etc. The litter fraction of total net production (i.e. the discarded fraction, *LF/NPP*) has been found to increase in more productive environments, especially in the tropics (Jordan 1971). Herbivory losses may also become larger fractions of *NPP* in the tropics.

In addition to respiration, vegetation also releases CO_2 to the atmosphere through decomposition of dead biomass. The total net energy (or carbon or CO_2) balance of a place, also called net ecosystem production, can be expressed as

$$\Delta C = GPP - R - D \quad (3)$$

where D is the total amount of detritus decomposed. Decomposer populations decompose litter pools (L, e.g. surface litter, below-ground root litter) at a fractional rate k (Olson 1963), as given by

$$D = k \cdot L \quad (4)$$

This rate k is primarily a function of climate and litter quality (Meentemeyer 1978, 1985; cf. Whitford *et al.* 1981).

The bioclimatic relationships described above generally control the productivity and some structural aspects of natural vegetation at regional to global scales (Major 1963; Rosenzweig 1968; Lieth 1975a, 1975b; Box 1978, 1981; O'Neill & DeAngelis 1981; Meentemeyer *et al.* 1982; Esser *et al.* 1982). As a result, climate-based models have been fairly successful at capturing the general global patterns of primary productivity and certain other aspects of vegetation dynamics (O'Neill & DeAngelis 1981). Such climate-based models, however, tacitly assume a vegetation cover which is 'natural', i.e. under climatic control. At more local scales, vegetation structure and productivity are controlled jointly by climate and more local factors, including local soils and topography, nutrients, vegetation history, disturbance regimes, and agricultural or other human land use. In such situations, satellite data may provide better indices than climate-based models, since the satellite data represent the actual rather than potential vegetation cover.

Methodology and data

This evaluation of the *NDVI* involves both field measurements and simulation results at particular sites. Simulation results are included since they permit better geographic coverage (about 10 times as many sites) and permit study of gross production and respiration, for which there are very few direct measurements. The analysis is statistical, despite the spatial autocorrelation of geographic data. This analysis, however, seeks only general relationships and so is valid as long as one understands its statistical limitations.

The data include measurements of primary production and biomass at discrete field sites, climatic data for these and many more simulation sites, and spatially corresponding *NDVI* pixel values and images derived from the *GVI* (Global Vegetation Index) data-base described by Tarpley *et al.* (1984). The biological measurements were made during the International Biological Program (1964–1974) and afterwards but still involve only about 130 sites with both above and below-ground biomass and *NPP* for quasi-natural vegetation. The measurements represent a variety of methods, from harvesting at intervals to allometric estimates, but have been interpreted and standardized as far as possible, mainly by DeAngelis *et al.* (1981) and by Cannell (1982). Most major vegetation types are represented, covering the full range of bioclimates. The production measurements are for one year each, due to the large amount of time and work involved in the measurement procedures. Despite shortcomings, these are the only measurements of primary production available to us. Site vegetation descriptions and basic climatic data were added and measurements re-checked, based on the original literature.

In addition to the biological measurements, a global climatic data-base of monthly temperature and precipitation values ($n=1596$ sites) was employed for more complete geographic coverage using bioclimatically simulated metabolic values. These climatic stations were chosen for good representation of global physiography and had been used for world maps of primary productivity, litter dynamics, net ecosystem CO_2 flux, etc. (e.g. Lieth 1975; Box 1978, 1981, 1988; Meentemeyer *et al.* 1982). Potential (*PET*) and actual evapotranspiration (*AET*) estimates were generated for these climate sites by means of climatic water-budget procedures, based on a geographically improved estimator for global *PET* (Box 1979, 1982, 1986). In order to minimize artifacts, annual *NPP* is estimated by averaging the values given by two earlier climate-based *NPP* models (Lieth & Box 1972). Annual *GPP* and *R* are estimated from annual *NPP* (Lieth & Box 1977) and are then partitioned bioclimatically to yield estimates of monthly *GPP*, *R* and "*NPP*" (which may become negative, cf. equation 1).

The rest of the energy (carbon) balance of the vegetation-detritus system, including the net ecosystem CO_2 flux, by months, is estimated by a climate-based simulation model described elsewhere (Box 1988). We are forced to rely on this model, it being the only model which can provide relatively detailed global geographic patterns for all the main carbon-balance components (equations 1, 3, 4) – in biological units, as appropriate for satellite calibration. This model is based on global, geographically representative measurement sets, has been tested in a variety of ways (cf. Gillette & Box 1986; Box in press), produces reasonable geographic patterns of carbon-budget components, apparently including the relatively sensitive CO_2 source-sink balance (cf. Houghton 1987b; Box 1988), and produces consistent results under somewhat differing model formulations.

For global *NDVI*, the best currently available product is the *GVI* data-base, which covers 34 consecutive months during 1982–1984 and has been used for most previous *NDVI* work. The pixel size varies from about 15 km at the equator to around 30 km at high latitudes. Raw *NDVI* pixel values range from 0 to 1024 counts, with lower values indicating more greenness. These raw values are inverted and re-scaled to the range 0–1 by the formula

$$\text{scaled } NDVI = ((961 - \text{raw } NDVI)/1401) - 0.5 \quad (5)$$

which places zero greenness at $NDVI=0$ and maximum greenness at $NDVI=1$. The highest *NDVI* encountered in either global data-base was 0.391, hence an asymptote value of $NDVI=0.4$ in the subsequent models.

Because of the wide swath of the AVHRR and frequent passes by the NOAA-7 satellite, relatively cloud-free spectral coverage can be obtained for enough days each month to construct valid monthly *NDVI* composites for continents and the whole world, based on maximum values. This maximum-value compositing is described and evaluated by Holben (1986). Monthly composites represent current greenness but can also be integrated annually to give estimates of total annual greenness duration. Annually integrated *NDVI* is the annual sum of the monthly *NDVI* values, re-scaled to the same 0–1 range.

Monthly and annual *NDVI* pixel values corresponding to the biosphere measurement and simulation sites were extracted individually from the *GVI* images based on an algorithm which compares the target pixel with all adjacent pixel values. If the target pixel had an unreasonable value, it could sometimes be replaced by an appropriate average of adjacent values. Pixels dominated by ice caps, ocean, terrestrial water bodies or wetlands, or other inappropriate surface features yield unreasonable but recognizable raw *NDVI* values and could not be used.

The remaining *NDVI* pixel values were added to the biological data-bases, now reduced to 113 measurement sites and 1021 simulation sites with valid corresponding pixel data. Each site in the two data-bases was next given six one-character codes describing the altitudinal belt (if not lowland), unusual topographic features (coastal, saltflat, etc.), vegetation cover, and important land uses (especially irrigation in dry climates). The vegetation cover (see Table 1) is described by three codes representing the main plant types, seasonality (evergreen, deciduous, etc.), and landscape type (forest, open woodland, etc.). About 50 vegetation formation types and subtypes are obtained by combining these three codes. This system provides a flexible, fairly complete description of vegetation structure and cover degree, and can be converted to a more familiar classification structure by treating the codes hierarchically. This approach is based on the physiognomic classifications of Mueller-Dombois & Ellenberg (1974, Appendix B) and Box (1981), with bioclimatic affinities suggested by basic climate types according to Walter (1968, 1973, 1984). Altitudinal belts are defined ecologically, based on vertical changes in vegetation type. The other codes were determined from study of regional and local vegetation and topographic maps as well as field experience in many of the areas involved.

The resulting data-bases are very powerful, being the first global data-bases to combine site biosphere values with valid satellite data at the same locations. One shortcoming is that the biotic, climatic, and satellite data could not be made temporally concurrent. This problem is ameliorated by using three-year averages of the monthly AVHRR data and climatic data averaged over many years. In one geographic study involving multi-year biological data, it was found that annual litterfall totals vary from year to year but do not appear to be more closely related to current-year climate than to long-term average climatic conditions (Slota 1985). Future applications of satellite data will certainly involve real-time and near-future predictions, which will permit closer study of such year-to-year variabilities.

Global NDVI patterns

The first step in analyzing the *NDVI* was to attempt to understand how much pixel greenness varies and how it may be affected by regional biases and/or unusual surface features. Theoretical considerations, the time component, and initial statistical results suggested that the biosphere variables most closely related to annually integrated *NDVI* should be annual totals for integrative processes, in particular actual evapotranspiration (*AET*) and primary production. *AET* is a commonly used general ecological index (Carter & Mather 1966; Mather 1974; Meentemeyer *et al.* 1982) integrating simultaneous warmth and soil water availability (assuming a vegetation cover). *AET* has been found to be well correlated with primary production (Lieth & Box 1972), litter production and decomposition rate (Meentemeyer 1978, 1985), some vegetation types (Mather & Yoshioka 1966), and some other biosphere phenomena (e.g. Brook *et al.* 1983). Since primary production is simulated from *AET* in global models and may involve factors other than climate, annual *AET* appeared to be the most closely related biosphere variable for which the larger global data-base could confidently be used.

Scattergrams and theory both suggest that annual greenness duration should increase, geographically, as *AET* increases, but with an upper limit posed by effective foliage deployment and the spectral properties of the foliage. This means a saturation curve, passing through the zero-zero point and with an upper asymptote. This initial global trend relationship was quantified by transformed linear regression (SAS 1986) and refined (by removing obviously abnormal pixels) to yield the equation shown here and in Fig. 1:

Table 1. Vegetation cover types and codes for the measurement and simulation data-sites.
The vegetation cover at each site is described by a system of three one-character codes representing the main plant types, seasonality, and landscape type, as described in the main text. The vegetation formation types, which result from combining these three codes, represent the actual vegetation over larger areas. Thus, where natural or semi-natural vegetation is more or less completely replaced by artificial landscapes, secondary vegetation may be coded instead of the potential natural vegetation. Vegetation types at the particular sites were determined from various regional vegetation maps (Schmithüsen 1976; Küchler 1964; Eyre 1968; Hueck & Seibert 1972; Rowe 1972; Horvat *et al.* 1974; UNESCO 1969; Hou *et al.* 1980; Beard 1980; UNESCO 1981a, 1981b), plus field experience. Monthly sequences of *NDVI* values were checked in order to correct gross errors in vegetation seasonality, but this was done sparingly, in order to avoid logical circularity in subsequent analyses.

Abbreviations

Plant types:
BL = broad-leaved; EG = evergreen; decid. = deciduous

Seasonality:
E = evergreen; S = semi-evergreen; D = deciduous; .X = ephemeral

Landscape types:
D = desert; F = forest; G = grassland; I = ice cap
K = krummholz; S = semi-desert; T = tundra; V = savanna
W = woodland; X = scrub

Main plant types	Seasonality type	Landscape type	Vegetation formation types	Examples
Tropical BL-EG trees (1)	E	F	Tropical rainforest	Amazon Basin, E Indies
Tropical seasonal trees (2)	D,S	F,W	Tropical deciduous/semi-EG forest or woodland	India, miombo woodland
BL-EG trees (extra-trop.) (E)	E	F	Warm-temperate/subtropical laurel forest	S Japan, SE China
Semi-EG BL trees (S)	S	F,W	Humid subtropical forest, dry equatorial woodland	SE China, eastern Chaco; E Africa
Summergreen trees (6)	D	F,W	Temperate deciduous forest or woodland	E USA, central Europe; oak woods of NE China
Needle-leaved EG trees (N)	E	F,W	Boreal forest/woodland	Canada, Siberia
Mixed (decid. + needle) trees (M)	S	F	Subboreal and warm-temperate mixed forests	New England, Baltic USSR; SE USA (oak-pine)
Larch trees (L)	D	F,W	Larch forest/open woodland	Eastern Siberia
Mediterranean trees/scrub (4)	E,S,D	F,W,X	Mediterr. forest, chaparral, or dwarf-shrubs (garrigue)	Maquis, matorral, phrygana, fynbos, kwongan, etc.
Scrub (general) (X)	E,S,D	X	Mixed scrub, non-mediterranean shrublands, etc.	Thorn-scrub, shrub-woodlands, juniper scrub, etc.
Savanna (tropical) (V)	E,S,D	V	Tropical savannas	E Africa, sub-humid Australia
Grassland (G)	E,S,D	G	Temperate or montane grasslands and steppes	US Great Plains, Ukraine, S African veld, pampa
Treeline krummholz (N,M,6)	E,S,D	K	Subpolar and subalpine krummholz	Subpolar birch scrub; subalpine conifer krummholz
Tundra (subpolar) (9)	S,D	T	Tundra: typical (snow) and maritime (little snow)	N Canada and Siberia; Iceland and subantarctic islands
Tropical alpine (P)	E,S,D	X,G,S	Páramo, wet and dry puna	Andes, E Africa
Temperate arid (7)	S,D	X,S,D	Temperate desert/semi-desert	US Great Basin, Middle Asia
Extreme desert (D)	X,-	D	Subtropical/other true deserts	Sahara, Atacama, Takla Makan
Polar desert (9)	D	D	Polar cold-desert	High Arctic (snow-free summer)
Ice cap (no vegetation)	-	I	Ice cap (no vegetation)	Antarctica, Greenland

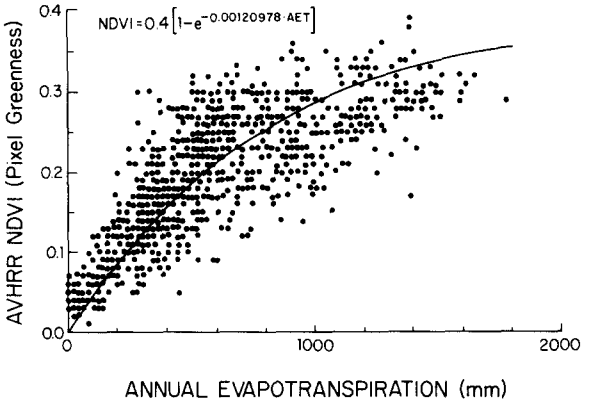

Fig. 1. Global trend of annually integrated *NDVI* and annual actual evapotranspiration. Theoretical considerations and initial statistical results both suggested that annually integrated *NDVI* might be closely related to annual totals of actual evapotranspiration (*AET*), with scattergrams and theory both suggesting a saturation relationship (with upper asymptote at *NDVI* = 0.4). This initial global trend relationship was quantified by transformed linear regression to yield the equation shown here. Greenness increases, geographically, as *AET* increases and is thus related to bioclimate. The reflectance behavior and validity for calibration use of the various data-sites, representing different kinds of vegetation, topography and land use, were evaluated initially by comparison with this global *NDVI-AET* relationship.

$$NDVI = 0.4\,[1 - e^{-0.00120978 \cdot AET}] \qquad (6)$$

where *AET* is in mm, the asymptote is based on the highest annual *NDVI* value (0.391) observed in either data-base, and the curve was forced through the zero-zero point (SAS redefined $r^2 = 0.87$). Since this relationship was derived from apparently normal pixels only, the reflectance behavior and validity of the data-sites can be evaluated initially by examining deviations above or below this global *NDVI-AET* trend curve.

Effects of particular topographic and land-use situations are summarized in Table 2. Alpine and subalpine areas are too small to represent full pixels accurately and were excluded immediately from further analyses. Coastal fjord and narrow valley sites show erratic *NDVI* values (poor lighting) and were also excluded. Lakeshore, river-valley, and saltflat sites in dry climates, as well as irrigated lands, fall consistently above the general trend (greener than their climates would suggest) and also cannot logically be used for calibration of *NDVI* values relative

Table 2. Relative pixel greenness of different topographic and land-use situations.
The reliability of *NDVI* values in different altitudinal belts and topographic and land-use situations was evaluated by comparison with the global *NDVI* trend curve (see Fig. 1), as described in the main text. The numbers of sites in the simulation data-base (n = 1021) having annual *NDVI* values above and below this global trend curve are shown here. Various situations fall consistently and anomalously above the general trend and were excluded from further analyses.

	All pixels (n = 1021)		Valid pixels (n = 947)	
	above	below	above	below
Altitudinal belts				
Lowland/upland	489	326	447	322
Montane	141	38	140	38
Subalpine	9	3	(excluded)	
Alpine	11	4	(excluded)	
Total	650	371		
Unusual topographic situations				
Desert (extreme, not irrigated)	16	0	16	0
Icecap (permanent)	7	0	7	0
Fjords, narrow valleys	2	4	(excluded)	
Lakeshores, river valleys, and saltflats in dry climates	9	0	(excluded)	
Significant land use				
Irrigated land (dry climate)	32	0	(excluded)	
Total valid pixels			587	360
Valid lowland pixels (vegetated, deserts excluded)			424	322

to climatic and biological measurements. Extreme desert and icecap pixels have low *NDVI* values, but these rarely fall completely to zero, probably due to background effects from the light-colored surfaces (Holben 1986). The *NDVI* is thus invalid at its extreme low end. These desert and icecap sites are retained, however, as necessary end-points of the *NDVI* and landscape spectrum. Of the remaining sites considered valid (n = 947), montane sites tend to show higher *NDVI* values than comparable lowland sites, still suggesting partly mixed pixels. When montane and desert sites are excluded, the numbers of remaining lowland pixels falling above (424) and

below (322) the upwardly convex trend curve are somewhat more evenly balanced.

Relationships of different landscape and some regional vegetation types to the global *NDVI-AET* pattern, for non-desert lowland sites only, are summarized in Table 3. At the level of general landscape types (forest, grassland, etc.), only the sparsely vegetated scrub and semi-desert types deviate significantly from the global pattern, generally showing enhanced greenness, probably due to background effects. At the level of particular vegetation types, however, tropical sites fall mainly below the global trend (less green than expected) while temperate-zone sites fall mainly above the trend curve (greener than expected). This imbalance may be exaggerated by the shape of the statistical regression curve, which passes above many high-*AET* sites but below many sites in the middle and lower *AET* range (cf. Fig. 1). On the other hand, close examination of the *NDVI-AET* scattergram suggests the possibility of two (or more) distinct statistical populations, possibly representing different patterns of spectral response in different regions or cover types. This cannot be explained here and requires further study.

Table 3. Relative pixel greenness of landscape and vegetation types.
For evaluation of the reflectance behavior of different vegetation cover types, only valid lowland sites are examined, as suggested in the main text. The numbers of sites above and below the globally derived *NDVI-AET* relationship (Fig. 1) are shown for the main landscape types plus some particular vegetation formation types. Sparsely vegetated landscapes (semi-desert, desert, etc.) all show more greenness than would be expected. More striking is that tropical sites tend to fall mostly below the global trend while temperate-zone sites fall mainly above the trend curve. Close examination of the *NDVI-AET* scattergram (Fig. 1) suggests the possibility of two (or more) distinct statistical populations, possibly representing different regional patterns of spectral response.

	Valid lowland pixels (n = 746)	
	above trend	below trend
Forests	168	148
Tropical rainforest	9	24
Tropical deciduous forest	8	40
Temperate deciduous forest	57	8
Boreal (evergreen) forest	50	27
Woodlands	100	72
Tropical woodlands	15	34
Temperate woodlands	85	38
Grasslands	44	59
Savannas (tropical)	8	35
Treeless (trop. and temp.)	36	24
Scrub/Krummholz	31	10
Tundra	12	11
Semi-deserts	69	22
Subtropical	54	19
Temperate	15	3
Total (Valid lowland pixels)	424	322

Apparently invalid situations were also deleted from the set of measurements, mainly some high-mountain or heavily grazed sites. Despite remaining minor anomalies, however, no other situations could be systematically excluded without impairing the global nature of both data-bases. The final data-bases, based on pixel and measurement validity, involve 95 measurement sites and 947 climate (simulation) sites.

Data ranges and median values for the main variables in both data-bases are summarized, by vegetation type, in Table 4. The global data-base (n = 947) appears to represent adequately the geographic and quantitative ranges of biomass and greenness variation. Simulated *NPP* values were generated by the models of Lieth & Box (1972) and generally fall within the ranges of the *NPP* measurements, despite variations in method, location, and year of measurement, etc. There are only 95 valid measurement sites, but this is double the 50 or fewer measurement sites available for earlier models. The measurements used herein span the full range of values known and provide some improved geographic representation, though some vegetation types remain poorly represented by actual measurements.

Greenness and primary productivity

Considering the temporal nature of annually in-

Table 4. Data ranges for biosphere measurement sites and global simulation coverage.
Numbers of valid sites and ranges of important biosphere variables and annual *NDVI* (× 1000) are shown for the biosphere measurement sites and the sites used to simulate global patterns of biosphere features. The values are shown by vegetation formation type (biome), based on classification of all sites available (see Table 1). All values on the left represent field measurements (*LAI* = Leaf Area Index), while all values on the right (including median *NPP*) represent estimates based on models. The ranges of annually integrated *NDVI* are based on all sites in the simulation data-base (n = 947), which generally showed wider ranges of annual *NDVI* than did the set of measurement sites. Productivity, *AET*, and greenness (*NDVI*) generally decrease toward the poles (for forests) or toward drier environments. Forests, tundra, and deserts/semi-deserts generally show smaller ranges of annual *NDVI* values, with larger ranges for scrub and grassland types. (Note that only 91 measurement sites are listed. The other four represent substitute vegetation: three treeless tropical grasslands and one British moorland.)

Biome	Measurement sites (valid, n = 95)				Global simulation (valid pixels, n = 947)				
	No. of sites	Biomass (kg/m²)	*NPP* (g/m²/yr)	*LAI*	No. of sites	*AET* (mm/yr)	Median *NPP* (g/m²/yr)	Median *GPP* (g/m²/yr)	Annual *NDVI* (× 1000)
Tropical forests									
Rainforest (evergreen)	7	32 – 56	1273 – 3101	9 – 12	33	850 – 1650	2100	6000	392 – 272
Deciduous	2	24 – 74	930 – 2665	–	50	600 – 1475	1700	4400	340 – 173
Semi-evergreen	1	20	1260	4	43	700 – 1500	1900	4600	361 – 196
Temperate forests									
Evergreen broad-leaved	1	39	1000	4	34	500 – 1400	1500	2500	328 – 151
Deciduous broad-leaved	17	11 – 37	864 – 1900	3 – 7	65	500 – 900	1400	2600	301 – 166
Semi-evergreen (broad)	0	–	–	–	10	500 – 1200	1600	3200	268 – 152
Evergreen conifer	9	11 – 85	650 – 2487	5 – 12	22	300 – 1100	1200	2400	300 – 115
Mixed (broad + conifer)	2	10 – 65	1196 – 1484	4 – 9	90	400 – 1250	1350	2800	324 – 143
Boreal forests/woodlands									
Evergreen conifer	8	3 – 28	92 – 719	2 – 10	100	175 – 500	700	1150	217 – 81
Deciduous (larch)	1	21	1713	7	25	80 – 450	450	700	200 – 73
Woodlands (non-boreal)									
Tropical deciduous	0	–	–	–	28	680 – 1160	1600	3200	327 – 111
Mixed tropical	1	11	3340	1	27	470 – 1350	1500	3100	320 – 216
Sclerophyll	1	3	403	2	23	425 – 960	1150	2100	316 – 141
Mixed extra-tropical	0	–	–	–	54	200 – 910	1000	1800	253 – 103
Conifer (evergreen)	0	–	–	–	6	360 – 710	900	1500	295 – 147
Scrub									
Tropical-subtropical	0	–	–	–	19	300 – 785	1000	1600	318 – 83
Mediterranean-type	3	3 – 8	302 – 1981	2 – 3	18	275 – 560	800	1500	299 – 58
Temperate arid	0	–	–	–	19	140 – 410	550	900	233 – 68
Subpolar krummholz	2	3 – 4	71 – 198	–	1	250	550	800	157
Grasslands									
Tropical savanna	5	0.6 – 7.1	410 – 3455	(0.1 – 0.4)	47	400 – 975	1200	2300	304 – 52
Temperate grasslands	9	0.3 – 3.3	296 – 1425	–	85	165 – 800	900	1500	264 – 77
Tundra									
Typical tundra	12	0.2 – 2	7 – 281	(0.1)	20	50 – 275	300	450	101 – 27
Maritime tundra	0	–	–	–	3	285 – 425	450	800	136 – 65
Semi-desert									
Subtropical	1	–	950	–	80	25 – 385	400	550	201 – 13
Temperate	8	0.8 – 3.4	125 – 396	–	21	25 – 200	250	350	108 – 19
Desert (extremely arid)	1	0.004	4	–	17	0 – 20	10	15	69 – 21
Icecap (permanent)	0	–	–	–	7	0 – 2	0	0	31 – 29

tegrated *NDVI*, it seems that it must be more closely related to process rates or totals than to structural features, such as biomass amounts. Sharp *et al.* (1974) found a global relationship between annual *NPP* and growing-season length, and in a sense annually integrated *NDVI* represents the amplitude of the growing season.

Annually integrated *NDVI* is plotted in Fig. 2 against the 95 valid measurements of annual *NPP*, with symbolism for the different vegetation types. Linear regression yielded an unrestrained *r*-value of 0.713, but the plot suggests a slightly saturating relationship, similar to that of Goward *et al.* (1985) and for *AET* (Fig. 1). This relationship was quantified by transformed linear regression as a saturation equation (redefined $r^2 = 0.81$) with upper asymptote at *NDVI* = 0.4, as for equation 6. Equatorial rainforests, polar tundras, and deserts, as three environmental extremes, largely define the overall trend of the *NDVI-NPP* relationship. (These environments are also more likely to be relatively undisturbed over the area of whole pixels.) Some of the highest *NPP* values belong to tropical C_4 grassland sites, with relatively lower greenness values.

Plots of annual *NDVI* versus the above-ground ($r = 0.64$) and below-ground ($r = 0.35$) fractions of annual *NPP* showed similar curvilinear patterns but with wider scatter, especially for the below-ground component (plots not shown). Below-ground *NPP* is sometimes estimated based on above-ground *NPP* and root-shoot ratios, so the poorer relationship for below-ground *NPP* probably reflects the unreliability of some data.

For more complete global coverage, annually integrated *NDVI* is plotted against climatically simulated annual *NPP* in Fig. 3. In regression of *NDVI* against *NPP*, the unrestrained linear model yielded a higher correlation coefficient ($r = 0.835$ vs. 0.799) than did a saturation form (cf. Fig. 2). The scattergram, however, still suggests an upper limit to surface greenness, and basic ecological theory requires a zero-point (no greenness at zero *NPP*). This and the result for the measurement sites (Fig. 2) suggest that the saturation form is still the better general model.

Because curve fitting smooths the actual *NPP* values, the correlation coefficient for *NDVI* is higher against simulated *NPP* ($r = 0.835$) than against the

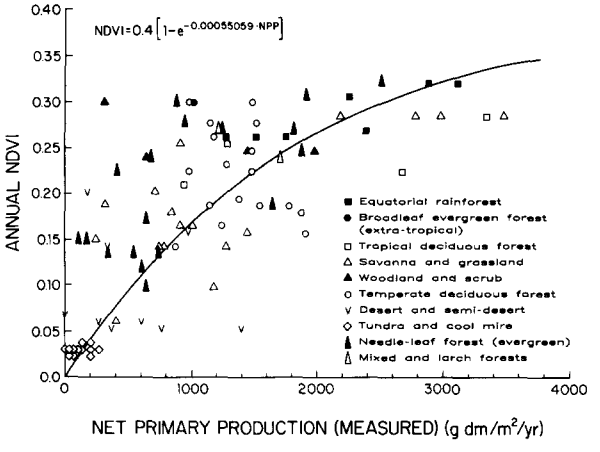

Fig. 2. Data and relationship between annually integrated surface greenness (*NDVI*) and annual net primary production (*NPP*), based on measurements from different biomes ($n = 95$). The site measurements involve relatively natural vegetation representative of the corresponding pixels and free from major disturbances. *NPP* values are expressed in g dry matter · m^{-2} · yr^{-1}. The scattergram pattern suggests a saturation relationship between greenness (*NDVI*) and *NPP*, as was seen for actual evapotranspiration (Fig. 1). This was quantified by transformed linear regression using the same asymptote (*NDVI* = 0.4) as for the *NDVI-AET* relationship, based on the highest *NDVI* value in the global data-base.

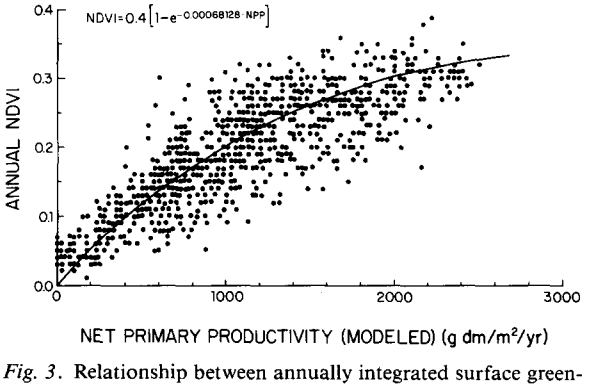

Fig. 3. Relationship between annually integrated surface greenness (*NDVI*) and climatically simulated annual net primary productivity (*NPP*), from the global data-base ($n = 947$). For more complete global coverage, annually integrated *NDVI* is compared here with climatically simulated annual *NPP* (Lieth & Box 1972), without vegetation symbols. Despite a slightly higher *r*-value for a linear relationship (slope 0.0001656), the scattergram still suggests an upper limit to surface greenness, and basic ecological theory requires a zero-point (no greenness at zero *NPP*).

NPP measurements (r = 0.713). This suggests the importance of vegetation structure and history, spatial and temporal variability in production amounts, and perhaps significant error in some of the field measurements. This also illustrates the value of pooling many individual measurements to make more general world models. The correlation between annual *NDVI* and simulated annual *NPP* (linear, r = 0.835) is slightly stronger than that between annual *AET* and annual *NPP* measurements (r = 0.81, n = 53) in the curvilinear model by Lieth & Box (1972). The linear correlation between annual *NDVI* and measured net production (r = 0.713) is weaker than this earlier *NPP-AET* relationship but may improve with finer pixel dimensions.

Linear correlations of annually integrated *NDVI* versus climatically estimated annual *GPP* (r = 0.780) and respiration (r = 0.725) were also high but less than for *NPP*. For respiration this seems reasonable, due to the more rapid increase of respiration with temperature than for *GPP* or *NPP*. The lower correlation for *GPP* than for *NPP* may be statistical or may reflect data or modeling inadequacies and cannot be judged at this time.

Greenness and biomass structure

Annually integrated *NDVI* is plotted against measured total standing biomass in Fig. 4. The scatter of the data (linear r = 0.55) suggests at best only a limiting relationship. Grasslands and certain other low-biomass landscapes can appear quite green, while certain high-latitude and deciduous forest areas can have moderately high biomass amounts but only modest annual *NDVI* totals. Furthermore, increased accumulations of biomass in forests may involve mainly wood and may not yield significant increases in greenness values. As a result, there does not seem to be any reliable relationship, across different vegetation structures, between standing biomass and annually integrated *NDVI*. At most, a boundary curve can be drawn, suggesting a possible upper limit to biomass accumulation for mature, mesic forest sites. Drier, younger, non-woody, and certain other landscapes must fall well to the left of this boundary curve.

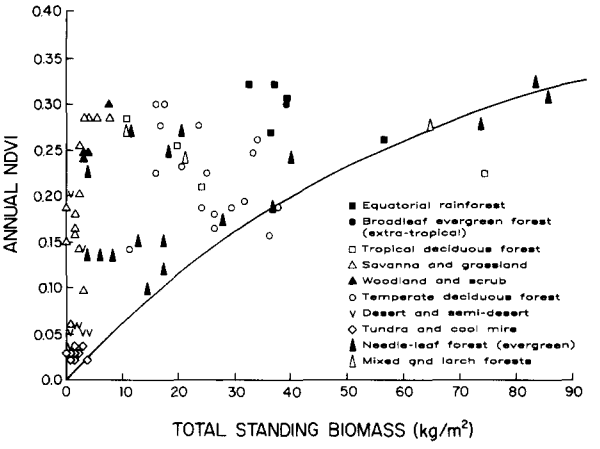

Fig. 4. Scattergram of annually integrated surface greenness (*NDVI*) versus total standing plant biomass, using measurements from different biomes worldwide (n = 93). The measurement sites (except for two without biomass data) and vegetation symbolism are the same as in Fig. 2. Biomass is expressed as kg dry matter (above and below ground) per m^2. The scatter of the data (linear r = 0.55) sugests at best only a limiting relationship, perhaps a potential upper biomass limit for mature mesic forests. Many sites, though, show significant greenness at much lower amounts of standing biomass. The curve was drawn by hand, as a boundary curve, and does not represent any statistical analysis.

Similar lack of any strong statistical relationship to annual *NDVI* was found for the above-ground and below-ground biomass components, their shoot-root ratios, and (seasonal maximum) leaf area index (see Table 5). These results seem altogether reasonable, since biomass structure has no real temporal component comparable to temporal *NDVI* integrations. On the other hand, leaf area duration may be related to annual *NDVI*, while monthly leaf area index may be related to monthly *NDVI* values. Further study of this requires more data.

Effects of vegetation type

Given the deviation geography (Tables 2 and 3) and the poor *NDVI*-biomass relationship (Fig. 4) across different vegetation structures, one might expect the validity of *NDVI-NPP* relationships also to show significant geographic variation or bias. In particular, bias due to vegetation structure might be expected with very tall, straight-growing trees, in which case leaf area may be closely related to height. Tall

Table 5. Correlations between annually integrated greenness and biosphere variables.
Linear correlation coefficients (r) are shown for annually integrated greenness (*NDVI*) versus annual primary production, biomass, and other biosphere variables, for both the measurement and simulation data-bases. Annual *NDVI* appears to be most closely related to annual primary production rates and actual evapotranspiration (*AET*). There appears to be no promising relationship, across the full range of biome types, between annual *NDVI* and shoot-root ratios, leaf area index, or biomass amounts. Relationships to total biomass may be worth pursuing, though, in some types of environments.

	Correlation coefficients (r) versus annual *NDVI*	
	Field measurements (n = 95 valid pixels)	Global simulation sites (n = 947 valid pixels)
NPP (total annual)	0.713	0.835
GPP (total annual)	-	0.780
Respiration (total annual)	-	0.725
NPP_a (above-ground annual *NPP*)	0.691	-
NPP_b (below-ground annual *NPP*)	0.350	-
Biomass (total standing)	0.550	-
B_a (above-ground biomass)	0.545	-
B_b (below-ground biomass)	0.523	-
Leaf area index (seasonal maximum)	0.234*	-
B_a/B_b (biomass shoot-root ratio)	0.044	-
NPP_a/NPP_b (*NPP* shoot-root ratio, annual)	0.301	-
B_a/B (above-ground biomass fraction)	0.344	-
NPP_a/NPP above ground *NPP* fraction, annual)	0.335	-
Actual evapotranspiration (total annual)	0.775	0.780

NPP = net primary production (or productivity, in simulations)
GPP = gross primary productivity
B = standing biomass
*n = 44 valid pixels

conifers can have extremely high leaf-area values (Waring *et al.* 1978) and may also have high annual *NDVI* values. Of 18 coniferous forests and woodlands shown in Fig. 2, eight fall well above the trend curve, indicating unusually high greenness relative to productivity. On the other hand, very tall conifers with extremely high leaf area can show enhanced productivity, as does also one tropical deciduous forest site (actually a large teak plantation with very tall trees, *NPP* = 2665 g/m^2/yr, but *NDVI* = only 0.23, see Fig. 2).

Most of the statistical operations were also run with separate data subsets for evergreen, deciduous, and semi-evergreen vegetation. Although major differences between seasonality subsets did not appear in the correlation results, one can notice a tendency (Fig. 2) for evergreen sites to fall above the trend curve more than deciduous sites do.

In order to assess the relative reliability of regional *NDVI* application, linear *NDVI-NPP* correlations were also run by vegetation type (see Table 6). (This involves only simulated *NPP*, since the measurement sites are too few for statistical treatment of subsets.) Note immediately that the regionalization reduces (unequally) the ranges of variable values and thus the resulting r-values, so that each lower level shows typically lower, more statistically sensitive r-values. Since this same statistical problem would be met in developing local *NDVI*-based models, these reduced r-values are perhaps useful warnings about the relative statistical sensitivity of different geographic regions and landscape groupings. Development of local *NDVI*-based models appears safer in more seasonal and in drier and/or colder environments with wider ranges of *NDVI* values (except extreme deserts, where *NDVI* values become erratic, see Table 4). Local *NDVI*-based models may be generally unreliable when restricted to less seasonal vegetation types, especially tropical or other evergreen forests.

Seasonal and high-latitude effects

Satellite-derived vegetation indices, once calibrated, can be used to estimate seasonal changes which may be very difficult to measure otherwise. Well-chosen monthly or other short-term observations at differ-

Table 6. Regional correlations between annually integrated greenness and simulated annual net productivity.
Linear correlation coefficients (r) between annually integrated greenness (*NDVI*) and simulated annual net primary productivity (*NPP*) are shown for different landscape types or groupings (i.e. sub-regions) in the global data-base. Reduction to regional scales reduces the ranges of the variables (though not uniformly), such that correlation coefficients become generally lower and more variable. This statistical problem and the resulting r-values suggest where *NDVI*-based regional predictions would be least reliable. The worst statistical relationships between *NDVI* and *NPP* appear in particular forest types (especially tropical) and in extreme deserts.

	n	*r*(*NPP*)
Forests	414	0.70
Evergreen	67	0.44
Tropical	33	−0.33
Temperate	34	0.32
Semi-evergreen	53	0.53
Deciduous	115	0.30
Tropical	50	0.06
Temperate	65	0.38
Mixed	90	0.34
Coniferous	82	0.66
Woodlands	196	0.76
Grasslands	132	0.43
Tropical savanna	47	0.51
Temperate grassland	85	0.52
Scrub/shrublands	56	0.57
Krummholz	1	-
Tundra	23	0.78
Semi-desert	101	0.60
Desert (extreme)	17	−0.37
Icecap (permanent)	7	-
Globe (valid pixels)	947	0.835

ent times of the year have been indispensable for distinguishing different vegetation types and may help in estimating biomass, seasonal dynamics, and some annual totals.

One potential obstacle to seasonal use of the *NDVI* involves the so-called terminator effect, i.e. the interruption of *AVHRR* signals during winter at high latitudes, due to low light levels and low sun angles (Holben 1986). This means that greenness (e.g. evergreen boreal conifer forests) cannot be seen in winter, which would appear to constitute a major problem for the global reliability of *NDVI*-based indices. On the other hand, for estimation of metabolic processes, this low-light artifact represents a fortuitous surrogate for the unfavorable winter climatic conditions and dormancy period at high latitudes. Even in highly maritime high-latitude areas (e.g. Iceland, subantarctic islands), where dormancy might be broken earlier due to less extreme cold, low light levels may still preclude significant net production and the error in annual *NDVI* totals would not be large relative to annual process totals.

A perhaps more serious high-latitude problem is the occurrence in springtime or early summer, at many sites above about 40° N/S, of one unreasonable monthly *NDVI* value, suggestive of a water surface. This may not greatly affect annually integrated *NDVI* except in polar situations with short growing seasons. This unreasonable *NDVI* value may be due to standing water from snowmelt but cannot be used and must be resolved before *NDVI* data can be used reliably for seasonal studies in high latitudes. In addition, the degree to which sufficient light for the *AVHRR* coincides temporally with the onset or ceasing of primary production during the transition seasons remains to be studied.

NDVI values were also compared with biosphere variables on a monthly basis, especially with *NPP*, *AET*, and the net ecosystem carbon (CO_2) balance. Monthly *GPP* and *R* were obtained from bioclimatic partitioning of annual values, while *NPP*, *D*, and ΔC were obtained from the more complete carbon-balance simulation. Because of opposing seasonal patterns, correlation values for the Northern and Southern Hemisphere separately are more meaningful than for the whole globe. Linear correlation coefficients are shown by month and hemisphere in Table 7.

Monthly *AET* correlations with *NDVI* show a nearly unimodal pattern in each hemisphere, with highest correlations in autumn. *NPP* (cf. eq. 1), on the other hand, shows weaker monthly correlation values than does *AET* and shows a bimodal pattern

Table 7. Monthly correlations between surface greenness and simulated biosphere variables.
Linear correlation coefficients (r) are shown for monthly greenness (*NDVI*) versus corresponding monthly actual evapotranspiration (*AET*) and simulated net primary productivity (*NPP*, actually *GPP* minus *R* as in equation 1) and net CO_2 exchange (ΔC, equation 3). Monthly *AET* correlations with *NDVI* show a nearly unimodal pattern in each hemisphere, while *NPP* shows weaker monthly correlation values and a bimodal pattern in each hemisphere. For monthly net CO_2 flux there appears to be little if any geographically consistent relationship to monthly *NDVI* values.

	Northern Hemisphere only (n = 735)			Southern Hemisphere only (n = 212)			Entire Globe (n = 947)	
	r(*AET*)	r(*NPP*)	$r(\Delta C)$	r(*AET*)	r(*NPP*)	$r(\Delta C)$	r(*AET*)	r(*NPP*)
January	0.73	0.38	−0.42	0.68	0.58	0.24	0.67	0.70
February	0.73	0.42	−0.37	0.71	0.61	0.26	0.82	0.70
March	0.69	0.53	−0.27	0.74	0.69	0.41	0.79	0.70
April	0.67	0.64	0.01	0.80	0.74	0.51	0.72	0.68
May	0.68	0.72	0.28	0.71	0.58	0.19	0.68	0.68
June	0.64	0.67	0.18	0.75	0.57	−0.03	0.69	0.70
July	0.60	0.57	−0.01	0.66	0.49	−0.08	0.67	0.64
August	0.58	0.51	0.05	0.58	0.40	−0.14	0.64	0.58
September	0.70	0.66	0.33	0.55	0.52	−0.02	0.68	0.66
October	0.79	0.74	0.47	0.62	0.61	0.08	0.76	0.71
November	0.79	0.66	0.29	0.67	0.68	0.27	0.81	0.75
December	0.73	0.54	−0.05	0.77	0.77	0.42	0.84	0.78
Annually	0.77	0.83	-	0.79	0.84	-	0.78	0.83

in each hemisphere, with strongest correlations in autumn and weakest correlations just after the solstices, especially in winter in the Northern Hemisphere (where *NPP* values are most likely to become negative). The lower late-summer correlation for *NPP* also seems reasonable, since increasing soil water stress and high respiration over the summer may reduce productivity before reducing the amount of foliage deployed (i.e. greenness).

Greenness and CO_2 flux

Overall ecosystem carbon balance and the net biosphere-atmosphere CO_2 flux (net ecosystem production) were summarized in equations 1–3. Monthly net carbon flux was simulated by the carbon-balance model used for this study (Gillette & Box 1986; Box 1988). In this equilibrium model, annual net carbon flux is constrained to be zero. The monthly CO_2 flux is typically positive (net uptake by vegetation) during the main growing season and negative (net CO_2 release) outside the growing season. In Table 7, however, there appears to be little if any geographically consistent relationship to monthly *NDVI* values, though relationships have been reported.

The monthly CO_2 flux estimates have been mapped globally (see Box 1988) and are used to compute the growing-season net flux (*GSNF*), which Fung *et al.* (1987) found to be related to annually integrated *NDVI*. Linear regression (n = 947) of annually integrated *NDVI* and the *GSNF*, however, yielded only r = 0.46, suggesting the importance of the seasonal coincidence of gross production and respiration noted by Houghton (1987a). In a scattergram with vegetation symbolism (not shown), the *GSNF* showed especially low values (relative to high *NDVI* values) in higher-latitude, montane, and equatorial forests. Highest *GSNF* values were seen in tropical deciduous and semi-evergreen forests, woodlands, and savannas.

In order to illustrate at least some of these relationships graphically, North American images of surface greenness (*NDVI*), actual evapotranspiration (*AET*), simulated net primary productivity (*NPP*, equation 1), and simulated net CO_2 flux (ΔC, equation 3) are shown in Fig. 5 for September, a month

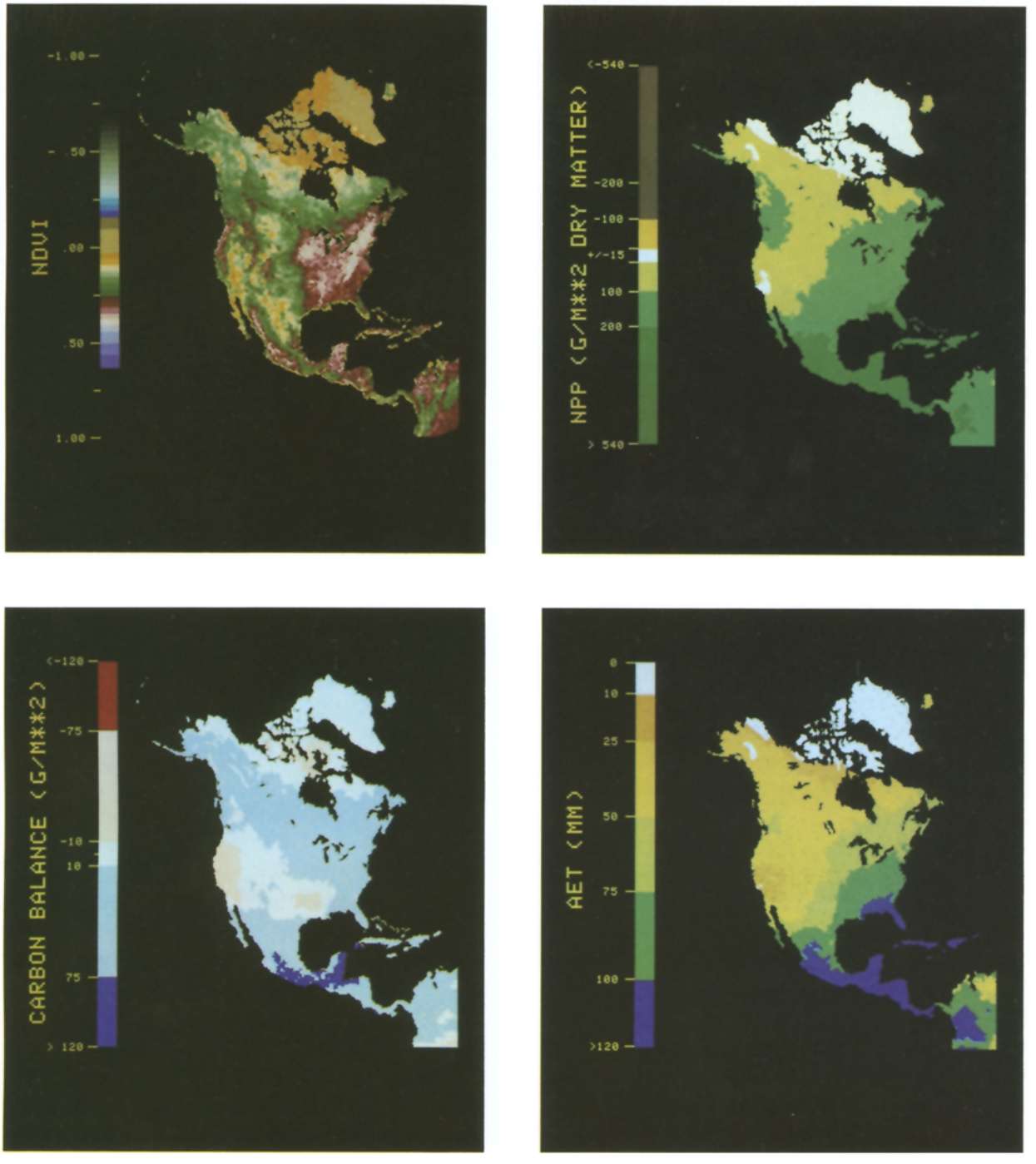

Fig. 5. Surface greenness (*NDVI*) and important biosphere patterns for September over North America. September geographic patterns for North America are shown for surface greenness (*NDVI*), actual evapotranspiration (*AET*), simulated net primary productivity (*NPP*, equation 1), and net CO_2 flux (ΔC, equation 3). *NDVI* seems to capture the main features of the continental patterns of *AET* and *NPP* and would appear to show promise as a general ecological index across the full range of ecosystem types. The *NDVI* does not, however, capture much of the geographic pattern of net CO_2 flux, due to its more sensitive balance between photosynthesis (CO_2 uptake) and respiration and decomposition (CO_2 release). September, as a transitional month, well illustrates the full range of values of the *NDVI* and each biosphere variable, but similar results were seen in other months.

with relatively high correlation between the *NDVI* and the biosphere variables. The September *NDVI* represents the average of values for 1984–1986 (actual surface vegetation), while *NPP* and ΔC are based on long-term climatic data (representing potential steady-state conditions). This difference is minimized somewhat by the use of North America, a relatively less disturbed continent.

Despite these temporal differences, the *NDVI* seems to capture much of the geographical patterns of September *AET* and *NPP*, including the latitudinal trend, the differences between humid east and summerdry west (USA), and the brief, late-summer monsoon season in the subtropical desert region. The *NDVI* does not, however, capture much of the geographic pattern of net CO_2 flux. In Table 7, net CO_2 flux shows mostly low or even negative correlations to monthly *NDVI*, throughout the year and in both hemispheres. Although monthly *NDVI* has been seen as correlated with monthly atmospheric CO_2 concentrations (Tucker *et al.* 1986) and surface CO_2 fluxes (Fung *et al.* 1987) at particular sites, it does not appear that the *NDVI* is consistently related to net ecosystem CO_2 flux across different biomes world-wide.

The sensitivity of the net CO_2 flux is illustrated in Fig. 5, in which a CO_2 source region ($R + D > GPP$) occurs in the south-central USA while a weak CO_2 sink or near balance between *GPP* and $R + D$ covers the rest of the deciduous forest region of the eastern USA. This initially surprising pattern seems to be caused by two climatic (and thus metabolic) gradients, an east-west dryness gradient (lower *GPP* to the west) and a north-south temperature gradient (higher respiration to the south), resulting in net CO_2 loss in the pink area in the south central USA. This result is not seen by looking at individual processes or the *NDVI*.

The individual processes which make up the total net CO_2 flux (equation 3) may or may not be in phase with each other in different biomes, varying in particular with evergreen versus deciduous vegetation (Box in press). This results in a more sensitive CO_2 source-sink pattern, but the locations of the main source/sink core regions have been relatively consistent in different model simulations.

Conclusions

1. *NDVI* values based on the current *GVI* product are not reliable in areas of complex terrain (high mountains, coastal areas, irrigated areas in dry climates, etc.) due to mixed pixels. The *NDVI* also does not fall to zero in vegetationless deserts or over snow cover, due to background effects. Current *NDVI* data seem to be reliable elsewhere, at least for annually integrated totals.

2. Relative to the general global pattern (represented by a global *NDVI-AET* trend curve), montane and temperate mesic wooded sites tend to show higher annual *NDVI* values than comparable lowland and tropical wooded sites; non-wooded sites (except tropical savannas) generally also show elevated *NDVI* values relative to the global trend.

3. The *NDVI* seems most closely related to primary production (or productivity), both net and gross, with a predictive accuracy for annual *NPP* comparable to that of climate-based *NPP* models. The *NDVI*-productivity relationship appears to be consistent worldwide.

4. The *NDVI* is also closely related to actual evapotranspiration (*AET*), corroborating earlier *AET*-based models of primary productivity.

5. There seems to be little reliable relationship between annually integrated *NDVI* and biomass amounts or structure across different biomes.

6. Sites with evergreen vegetation, especially tall evergreen conifer forests, appear to have somewhat higher *NDVI* values than deciduous sites. No other consistent structure-based bias was evident. An apparent tropical/extra-tropical bias cannot be explained at this time.

7. The high-latitude terminator effect, due to low sun angles in winter, does not seem to preclude reliable *NDVI*-based estimates of annual *NPP* or *AET* in boreal areas. Monthly *NDVI* values in high latitudes are less reliable, especially in springtime. This currently precludes use of the *NDVI* to study springtime phenology in high latitudes.

8. The *NDVI* seems to represent seasonality in net primary production and actual evapotranspiration. As Thomas & Henderson-Sellers (1987) recently remarked, however, it is difficult to incorporate this into a global model because the characterization and

quantitative relationships are not consistent globally.

9. There seems to be little reliable relationship across different biomes between the *NDVI* and net ecosystem production (CO_2 flux), either annually or monthly, due to seasonality effects and the sensitivity of the net CO_2 balance.

The above results represent the first rigorous demonstration that satellite-based ecological indices can be quantitatively related, consistently over the whole globe, to biosphere measurements at particular sites and to ground-based site indices, such as actual evapotranspiration and potential primary productivity. This ability to link satellite data, model results, and the types of measurements normally made by field biologists, at particular sites but consistently over different biomes, is important and provides confidence that more sophisticated, satellite-based models of biosphere phenomena can be developed. Generalized regional productivity assessments have been attempted in some areas (Sharp *et al.* 1976; Turner 1987) and should also be compared with satellite data. Improved *NDVI* coverage, with finer pixel dimensions and fewer errors, is needed and warranted by the potential accuracy and range of applications.

These results, however, also demonstrate the nature and magnitude of errors and obstacles involved in generalizing both satellite and field data. Satellite data will become more reliable as finer pixel dimensions are attained, reducing the mix of surface types in each pixel. It will be more difficult, however, to improve the biological field measurements without a general commitment to increasing the number, duration, and accuracy of production and biomass measurements, including below-ground components. More and better biological measurements are needed from all biomes, but especially from drier and more variable environments. A program for improving and standardizing such field measurements, and then re-assessing what we really know about biosphere metabolism and how accurately, is needed in order to improve our monitoring and modeling capabilities.

Acknowledgements

This work and publication costs were supported by grants NAG-5-516 and NAGW-1338 from the National Aeronautics and Space Administration to the first author. Statistical and modeling work were done, at the University of Georgia, but mapping was moved to the NASA Goddard Space Flight Center, where the color images were produced. The authors would like to thank C. J. Tucker and B. Choudhury for assistance and helpful suggestions.

References

AIBS 1986. Special issue on remote sensing of the biosphere. Bio-Science 36: 429–483.

Beard, J. S. 1980. Vegetation survey of Western Australia. 7 vols + maps (7 sheets). Univ. Western Australia Press, Nedlands.

Botkin, D. B., Estes, J. E, MacDonald, R. M. & Wilson, M. V. 1984. Studying the earth's vegetation from space. BioScience 34: 508–514.

Box, E. O. 1978. Geographic dimensions of terrestrial net and gross primary productivity. Radiat. Env. Biophys. 15: 305–322.

Box, E. O. 1979. World map of difference between Thornthwaite and Holdridge PET estimates. In: Harvard Library of Computer Mapping, 5: 11–27 (map 7). Harvard University, Cambridge (Massachusetts).

Box, E. O. 1981. Macroclimate and plant forms: An introduction to predictive modeling in phytogeography. Tasks for Vegetation Science, 1. Junk, The Hague.

Box, E. O. 1982. SOLWAT: A minimal-input soil water simulation system applicable to a full range of natural situations. Univ. of Georgia, Geography Dept., Athens.

Box, E. O. 1986. Some climatic relations of the vegetation of Argentina, in global perspective. In: Eskuche, U. & Landolt, E. (eds), Contributions to Knowledge of the Flora and Vegetation of Northern Argentina, Veröff. Geobotan. Inst. Rübel 18: 181–216.

Box, E. O. 1988. Estimating the seasonal carbon source-sink geography of a natural, steady-state terrestrial biosphere. J. Appl. Meteorol. 27: 1109–1124.

Box, E. O. 1988. Effects of seasonal vegetation structure on carbon dynamics of terrestrial biosphere models. In: Verhoeven, J., *et al.* (eds), Effect of vegetation structure and composition on carbon and nutrient economy. SPB Academic Publ., The Hague.

Brook, G. A., Folkoff, M. E. & Box, E O., 1983. A world model of soil carbon dioxide. Earth Surface Proc. Landforms 8: 79–88.

Cannell, M. G. R. 1982. World forest biomass and primary production data. Academic Press, London.

Carter, D. B. & Mather, J. R. 1966. Climate classification for environmental biology. Publ. in Climatology, 19(4), Univ. of Delaware.

DeAngelis, D. L., Gardner, R. H. & Shugart, H. H. 1981. Productivity of forest ecosystems studied during the IBP: the woodlands data-set. In: Reichle, D. E. (ed.), Dynamic properties of forest ecosystems, pp. 567–672. Cambridge University Press.

Dwivedi, R. 1971. Suitability of measuring carbon assimilation rates for evaluation of solar energy conservation and dry-matter production in plants. Trop. Ecol. 12: 123–132.

Esser, G., Aselmann, I. & Lieth, H. 1982. Modelling the carbon reservoir in the system compartment "Litter". SCOPE/UNEP special vol. 52, Mitteil. Geol.-Paläont. Inst. Univ. of Hamburg, pp. 39–58.

Eyre, S. R. 1968. Vegetation and soils, 2nd ed. Aldine, Chicago.

Fung, I. Y., Tucker, C. J. & Prentice, K. 1987. Application of advanced very high resolution radiometer vegetation index to study atmosphere-biosphere exchange of CO_2. J. Geophys. Res. 92(D3): 2999–3015.

Gillette, D. A. & Box, E. O. 1986. Modeling seasonal changes of atmospheric carbon dioxide and stable carbon isotopes. J. Geophys. Res., 91(D4): 5287–5304.

Goward, S. N., Tucker, C. J. & Dye, D. G. 1985. North American vegetation patterns observed with the NOAA-7 advanced very high resolution radiometer. Vegetatio 64: 3–14.

Holben, B. N. 1986. Characteristics of maximum-value composite images of temporal AVHRR data. Int. J. Remote Sens. 7: 1417–1434.

Horvát, I., Glavač, V. & Ellenberg, H. 1974. Vegetation Südosteuropas. Gustav-Fischer-Verlag, Stuttgart.

Hou Xue-yu *et al.* 1980. (Vegetation regions of the People's Republic of China.) Academia Sinica, Beijing (in Chinese).

Houghton, R. A. 1987a. Biotic changes consistent with the increased seasonal amplitude of atmospheric CO_2 concentrations. J. Geophys. Res. 92(D4): 4223–4230.

Houghton, R. A. 1987b. Terrestrial metabolism and atmospheric CO_2 concentrations. BioScience 37: 672–678.

Hozumi, K., Yoda, K. & Kira, T. 1969. Production ecology of tropical rainforests in southwestern Cambodia. II. Photosynthetic production in an evergreen seasonal forest. Nature and Life in Southeast Asia, 6: 57–81.

Hueck, K. & Seibert, P. 1972. Vegetationskarte von Südamerika. Vegetationsmonographien der einzelnen Großräume, vol IIa. Gustav-Fischer-Verlag, Stuttgart.

Johannsen, Ch. J. & Sanders, J. L. 1982. Remote sensing for resource management. Soil Conservation Soc. America, Ankeny (Iowa).

Jordan, C. 1971. A world pattern in plant energetics. Amer. Sci. 59: 426–433.

Justice, Ch. O. (ed.) 1986. Monitoring the grasslands of semi-arid Africa using NOAA-AVHRR data. Special number. Int. J. Remote Sensing 7: 1383–1622.

Justice, Ch. O., Townshend, J. R. G., Holben, B. N. & Tucker, C. J. 1985. Analysis of the phenology of global vegetation using meteorological satellite data. Int. J. Remote Sensing 6: 1271–1318.

Kira, T. 1975. Primary production of forests. In: Cooper, J. P. (ed.), Photosynthesis and productivity in different environments. Cambridge Univ. Press.

Küchler, A. W. 1964. The potential natural vegetation of the conterminous United States. Amer. Geogr. Soc., New York.

Kumar, M. & Monteith, J. L. 1981. Remote sensing of crop growth. In: Smith, H. (ed.), Plants and the daylight spectrum. Academic Press, New York.

Lieth, H. 1975a. Primary production of the major vegetation units of the world. In: Lieth, H. & Whittaker, R. H. (eds), Primary productivity of the biosphere, pp. 203–215. Springer-Verlag, New York.

Lieth, H. 1975b. Modeling the primary production of the world. In: Lieth, H. & Whittaker, R. H. (eds), Primary production of the biosphere, pp. 237–263. Springer-Verlag, New York.

Lieth, H. & Box, E. O. 1972. Evapotranspiration and primary productivity; C. W. Thornthwaite Memorial Model. Publ. Climatol. 25: 37–46, University of Delaware.

Lieth, H. & Box, E. O. 1977. The gross primary productivity pattern of the land vegetation: A first attempt. Trop. Ecol. 18: 109–115.

Major, J. 1963. A climatic index to vascular plant activity. Ecology 44: 485–498.

Mather, J. R. 1974. Climatology: fundamentals and applications. McGraw-Hill, New York.

Mather, J. R. & Yoshioka, G. 1966. The role of climate in the distribution of vegetation. Publ. Climatol. 19: 372–384, University of Delaware.

Meentemeyer, V. 1978. Macroclimate and lignin control of litter decomposition rates. Ecology 59: 465–472.

Meentemeyer, V. 1985. Climatic control of litter dynamics in tropical forest. In: Misra, K. C. (ed.), Ecology and resource management in tropics, pp. 302–310. Bhargava, Varanasi (India).

Meentemeyer, V., Box, E. O. & Thompson, R. 1982. World patterns and amounts of terrestrial plant litter production. BioScience 32: 125–128.

Moeller, C. M. 1945. Untersuchungen über Laubmenge, Stoffverlust, und Stoffproduktion des Waldes. Forstl. Forsoegsv. Danmark 17: 1–287.

Moeller, C. M., Mueller, D. & Nielsen, J. 1954. The dry-matter production of the European beech. Forstl. Forsoegsv. Danmark 21: 253–335.

Mueller-Dombois, D. & Ellenberg, H. 1974. Aims and methods of vegetation ecology. Wiley, New York.

Odum, E. P. 1971. Fundamentals of ecology, 3rd ed. W. B. Saunders Co., Philadelphia.

Olson, J. 1963. Energy storage and the balance of producers and decomposers in ecological systems. Ecology 44: 322–331.

O'Neill, R. V. & DeAngelis, D. L. 1981. Comparative productivity and biomass relations of forest ecosystems. In: Reichle, D. E. (ed.), Dynamic properties of forest ecosystems, pp. 411–449. IBP Series, Vol. 23. Cambridge University Press.

Rosenzweig, M. L. 1968. Net primary productivity of terrestrial communities: prediction from climatological data. Amer. Nat. 102: 67–74.

Rowe, J. S. 1972. Forest regions of Canada, revised ed. Dept. of Natural Resources, Ottawa.

Salisbury, F. B & Ross, C. W. 1978. Plant physiology. 2nd ed. Wadsworth Publ., Belmont (Calif.).

SAS 1986. Statistical Analysis System, version 5.16. SAS Institute, Cary (North Carolina).

Schmithüsen, J. 1976. Atlas zur Biogeographie. Bibliographisches Institut, Mannheim.

Sharp, D. D., Wyatt, R. E. & Lieth, H. 1974. Length of the growing period, in months (world map). In: Lieth, H. (ed.), Phenology and seasonality modeling. Springer-Verlag, New York.

Sharp, D. D., Lieth, H., Noggle, G. R. & Gross, H. D. 1976. Agricultural and forest primary productivity in North Carolina 1972–1973. N. Carolina Agric. Expt. Station. Techn. Bull. 241, Raleigh.

Shidei, T. & Kira, T. (eds) 1977. Primary productivity of Japanese forests. JIBP Synthesis series, Vol. 16, Tokyo.

Shugart, H. H. 1984. A theory of forest dynamics. Springer-Verlag, New York.

Slota, R. P. 1985. Climatic control of leaf litter production. M. A. thesis. University of Georgia, Athens (Georgia).

Tarpley, J. D., Schneider, S. R. & Money, R. L. 1984. Global vegetation indices from the NOAA-7 meteorological satellite. J. Clim. Appl. Meteorol. 23: 491–494.

Thomas, G. & Henderson-Sellers, A. 1987. Evaluation of satellite-derived land cover characteristics for global climate modelling. Climatic Change 11: 313–347.

Townshend, J. R. G. & Tucker, C. J. 1984. Objective assessment of advanced very high resolution radiometer data for land cover mapping. Int. J. Remote Sens. 5: 492–504.

Tucker, C. J. 1979. Red and photographic infrared linear combinations for monitoring vegetation. Remote Sens. Environ. 8: 127–150.

Tucker, C. J. 1980. A critical review of remote sensing and other methods for non-destructive estimation of standing crop biomass. Grass Forage Science 35: 177–182.

Tucker, C. J., Townshend, J. R. G. & Goff, T. E. 1985a. African landcover classification using satellite data. Science 227: 369–375.

Tucker, C. J., Vanpraet, C. L., Sharman, M. J. & Ittersum, G. 1985b. Satellite remote sensing of total herbaceous biomass production in the Senegalese Sahel: 1980–1984. Remote Sens. Environ. 17: 233–249.

Tucker, C. J., Fung, I. Y., Keeling, C. D. & Gammon, R. H. 1986. Relationship between atmospheric CO_2 variations and a satellite-derived vegetation index. Nature 319: 195–199.

Tucker, C. J. & Sellers, P. J. 1986. Satellite remote sensing of primary production. Int. J. Remote Sensing, 7: 1395–1416.

Turner, M. G. 1987. Land-use changes and net primary production in the Georgia (USA) landscape, 1935–1982. Environ. Management, 11: 237–247.

UNESCO 1969. Vegetation map of the Mediterranean zone. UNESCO, Paris.

UNESCO 1981a. Vegetation map of South America. UNESCO, Paris.

UNESCO 1981b. Vegetation map of Africa. UNESCO, Paris.

Walter, H. 1968. Die Vegetation der Erde in öko-physiologischer Betrachtung, Vol. 2: Die gemäßigten und arktischen Zonen. VEB Gustav-Fischer-Verlag, Jena.

Walter, H. 1973. Die Vegetation der Erde in öko-physiologischer Betrachtung, Vol. 1: Die tropischen und subtropischen Zonen, 3rd ed. Gustav-Fischer-Verlag, Stuttgart.

Walter, H. 1984. Vegetation of the earth. 3rd ed. Springer-Verlag, New York.

Waring, R. H., Emmingham, W. H., Gholz, H. L. & Grier, C. C. 1978. Variation in maximum leaf area of coniferous forests in Oregon and its ecological significance. Forest Science 24: 131–140.

Waring, R. H. & Schlesinger, W. H. 1985. Forest ecosystems: concepts and management. Academic Press, Orlando (Florida).

Whitford, W. G., Meentemeyer, V., Seastedt, T. R., Cromack, K., Crossley, D. A. jr, Santos, P., Todd, R. L. & Waide, J. B. 1981. Exceptions to the AET model: deserts and clear-cut forest. Ecology 62: 275–277.